Journal of Solid State Chemistry 184 (2011) 3232–3239

Contents lists available at SciVerse ScienceDirect

Journal of Solid State Chemistry

journal homepage: www.elsevier.com/locate/jssc

Cu–Ce–O mixed oxides from Ce-containing layered double hydroxide precursors: Controllable preparation and catalytic performance

Zheng Chang [a,*], Na Zhao [a], Junfeng Liu [a], Feng Li [a,*], David G. Evans [a], Xue Duan [a], Claude Forano [b], Marie de Roy [b]

[a] State Key Laboratory of Chemical Resource Engineering, Beijing University of Chemical Technology, Beijing 100029, China
[b] Laboratoire des Matériaux Inorganiques, UMR CNRS 6002, Université Blaise Pascal, 24 avenue des Landais, 63177 Aubière, France

ARTICLE INFO

Article history:
Received 5 May 2011
Received in revised form
26 September 2011
Accepted 28 September 2011
Available online 15 October 2011

Keywords:
Cu–Ce–O mixed oxides
Layered double hydroxides
Catalytic oxidation
Cu–Ce interactions

ABSTRACT

Cu/Zn/Al layered double hydroxide (LDH) precursors have been synthesized using an anion exchange method with anionic Ce complexes containing the dipicolinate (pyridine-2,6-dicarboxylate) ligand. Cu–Ce–O mixed oxides were obtained by calcination of the Ce-containing LDHs. The materials were characterized by X-ray diffraction, Fourier transform infrared spectroscopy, X-ray photoelectron spectroscopy, thermogravimetry–differential thermal analysis, elemental analysis, and low temperature N_2 adsorption/desorption measurements. The results reveal that the inclusion of Ce has a significant effect on the specific surface area, pore structure, and chemical state of Cu in the resulting Cu–Ce–O mixed metal oxides. The resulting changes in composition and structure, particularly the interactions between Cu and Ce centers, significantly enhance the activity of the Ce-containing materials as catalysts for the oxidation of phenol by hydrogen peroxide.

1. Introduction

Layered double hydroxides (LDH), also known as hydrotalcite-like compounds or anionic clays [1], can be represented by the general formula $[M^{II}_{1-x}M^{III}_{x}(OH)_2]^{x+}(A^{n-})_{x/n}\cdot yH_2O$. The identities of the divalent and trivalent cations (M^{II} and M^{III} respectively) and the interlayer anion (A^{n-}), together with the value of the stoichiometric coefficient (x), may be varied over a wide range, giving rise to a large class of isostructural materials [2]. After controlled thermal decomposition, LDHs lose their layered structure and form mixed metal oxides with high thermal stability, large specific surface area, and high metal dispersion, all of which are very important attributes for catalysts [3]. The resulting mixed metal oxides have been used as heterogeneous catalysts in many processes, such as hydrogenation, condensation, and oxidation reactions [4,5]. Compared with the materials prepared by conventional techniques (e.g. impregnation or precipitation), the catalysts derived from LDH precursors are generally characterized by higher activity and longer lifetimes [6].

Cu-containing LDHs, in particular, have been the focus of many studies because highly dispersed CuO is a well-known component of catalysts in many industrial reactions [7,8], such as catalytic wet oxidation (CWO) by air, oxygen, hydrogen peroxide or ozone [9]. Cu-based catalysts generally show high activity and have low cost, but suffer shortcomings such as leaching of the active centers and formation of a carbonaceous deposit [10]. Various methods have been employed to improve the performance of Cu-based catalysts, one of which is the addition of different metal elements such as Zr, V, Ce, and Mn [11,12].

Of these, Ce is widely regarded as a very effective additive for Cu-based catalysts [10,13]. For example, CuO–CeO_2 catalysts exhibit high activities in some oxidation reactions [14,15], even comparable to those of commercial noble metal catalysts. The catalytic materials therefore hold considerable promise for use in CWO of organic pollutants in water due to the relatively high abundance, as well as low cost of Cu and Ce [16]. Phenol is one of the most common organic species in wastewaters discharged from the petrochemical, chemical, and pharmaceutical industries. There have been many studies [17,18] on the application of CuO–CeO_2 catalysts in phenol oxidation, and there have been reports that their catalytic performance is even better than some commercial catalysts, such as $CuZnAlO_x$ [14]. The synergistic interaction between CuO and CeO_2 is thought to be the main factor responsible for the excellent catalytic properties [16,19]. The advantages of CuO–CeO_2 catalysts are mainly attributed to changes in the redox behavior of copper ions, the high dispersion of copper species, and the excellent oxygen storage capacity of the oxide systems [20–22].

One characteristic feature of the LDH structure is that there is a uniform dispersion of different ions at an atomic level within

* Corresponding authors. Fax: +86 10 64425385.
E-mail addresses: changzheng@mail.buct.edu.cn (Z. Chang), lifeng_70@163.com (F. Li).

0022-4596/$ - see front matter © 2011 Elsevier Inc. All rights reserved.
doi:10.1016/j.jssc.2011.09.035

the brucite-like layers, without the segregation of 'lakes' of like cations. Therefore the incorporation of Ce into Cu-containing LDH precursors, followed by controlled thermal decomposition should be a useful approach for the synthesis of $CuO–CeO_2$ catalysts with highly dispersed metal ions. However, the incorporation of a significant quantity of rare earth cations into the layers of LDHs is not feasible, because of the considerable mismatch between the radii of the large rare earth cations and the smaller Al^{3+}, Zn^{2+}, Cu^{2+} or other first row transition metal cations which typically form LDHs [23]. Rare earth cations readily form a wide range of anionic complexes with hard donor ligands, however, and subsequent intercalation of such anions into the interlayer galleries in Cu-containing LDHs is an alternative route for the preparation of rare earth-functionalized LDH materials [24,25]. We have previously described the intercalation of a series of pre-formed Ce^{3+} or Eu^{3+} complexes into Zn/Al-LDH materials and their luminescent properties [26,27].

In this work, preformed negatively charged tris(dipicolinato) complexes of Ce^{3+} have been intercalated by anion exchange into Cu/Zn/Al LDHs. The resulting LDH materials are transformed into Cu–Ce–O mixed oxides by calcination under different conditions and the performances of the different calcined materials in the catalytic wet oxidation of phenol have been compared.

2. Experimental

2.1. Sample preparation

A Cu/Zn/Al-LDH nitrate-intercalated precursor, denoted Cu-LDH, was prepared using a traditional titration process [28]. A mixed salt solution containing Cu^{2+}, Zn^{2+} and Al^{3+} nitrate salts with a 1/1/1 molar ratio was added dropwise to water in a flask, the solution being maintained at pH 7 by simultaneous addition of aqueous NaOH solution. The resulting suspension was stirred at 60 °C for 24 h. The procedure was conducted under a nitrogen atmosphere. The product was centrifuged, washed, and dried.

Tris(dipicolinato)cerium complex ($[Ce(dipic)_3]^{3-}$) was synthesized according to the method described in the literature [29]. A clear solution of disodium dipicolinate was obtained by stirring a mixture of pyridine-2,6-dicarboxylic acid (H_2dipic) (1.5 mmol in 50 mL of water) and NaOH (3 mmol in 25 mL of water). A solution of Ce(III) nitrate (0.5 mmol in 15 mL of water) was added slowly to the disodium dipicolinate solution. The pH value of the resulting solution was near 7. Slow evaporation at 30 °C gave prismatic crystals of $Na_3[Ce(C_7H_3NO_4)_3]\cdot xH_2O$ (x was generally ~15).

$[Ce(dipic)_3]^{3-}$-intercalated CuZnAl-LDH, denoted CuCe-LDH, was obtained by anion exchange of the NO_3^- anions of the host Cu-LDH by the $[Ce(dipic)_3]^{3-}$ complexes. The Cu-LDH powder was dispersed in deionized water for 24 h under flowing nitrogen and then added to the $[Ce(dipic)_3]^{3-}$ solution ($[Ce(dipic)_3]^{3-}/Al^{3+}$ molar ratio was 1/1 or 1/6). The resulting suspension was vigorously stirred for 24 h under a nitrogen atmosphere at room temperature. The products were recovered by centrifugation, washed with deionized water and dried in air. Finally, the mixed oxides were prepared by calcination in air at 500 °C or 700 °C for 3 h or 6 h. The synthesis parameters of all calcined samples, and the corresponding notation for each, are listed in Table 1.

For comparison purposes, a physical mixture of $Na_3[Ce(C_7H_3NO_4)_3]\cdot xH_2O$ and Cu-LDH with a Ce/Al molar ratio of 1/3 was synthesized and then calcined in air at 500 °C for 6 h; the resulting mixed oxide is denoted as Physical mixture-500-6. Commercial CeO_2 was calcined in air at 500 °C for 6 h, and physically mixed with pre-prepared Cu-500-6 (see Table 1) with a Ce/Al molar ratio of 1/3. The product is denoted as Cu-500-6 + CeO_2.

Table 1
The synthesis parameters for calcined LDH samples.

Samples	Initial Cu/Zn/Al/Ce molar ratio	Calcination temperature (°C)	Calcination time (h)
Cu-500-3	1:1:1:0	500	3
Cu-500-6	1:1:1:0	500	6
Cu-700-6	1:1:1:0	700	6
CuCe-500-3	1:1:1:1	500	3
CuCe-500-6	1:1:1:1	500	6
CuCe-700-6	1:1:1:1	700	6
CuCe6-500-3	6:6:6:1	500	3
CuCe6-500-6	6:6:6:1	500	6

2.2. Characterization

Powder X-ray diffraction (XRD) patterns were recorded on a Shimadzu XRD-6000 diffractometer under the following conditions: 40 kV, 30 mA, Cu $K\alpha$ radiation ($\lambda = 0.15418$ nm). The samples were step-scanned in steps of 0.08° (2θ) in the range of 3–70° using a count time of 4 s/step. In situ variable temperature XRD patterns were recorded using a Philips X' Pert PRO diffractometer equipped with an Anton Paar HTK16 high-temperature chamber and a PSD-50m Braun detector. Powders were deposited on Pt. Scans were recorded in air in the temperature range of 25–1100 °C with a heating rate of 5 °C/min and an equilibration time of 15 min before measurement at each temperature. Data were recorded in the range of 3–70° in continuous mode in steps of 0.04° (2θ). Fourier transform infrared (FT-IR) spectra were obtained on a Bruker Vector 22 spectrometer in the range of $4000-400\ cm^{-1}$ using the KBr pellet technique. Elemental analysis was performed using a Shimadzu ICPS-7500 inductively coupled plasma emission spectrometer (ICP-ES). Solutions were prepared by dissolving the samples in dilute nitric acid. The low temperature nitrogen adsorption–desorption experiments were carried out using a Quantachrome Autosorb-1C-VP system. Specific surface area was calculated from the adsorption branch according to the Brunauer–Emmett–Teller (BET) method. The pore size distribution was determined using the Barrett–Joyner–Halenda (BJH) model on the desorption branch. Prior to the measurements, samples were outgassed at 200 °C in vacuum for 3 h. The X-ray photoelectron spectra (XPS) were obtained with a Thermo ESCALAB 250 spectrometer (Al $K\alpha$, 200 W). The intensity of each peak was estimated by integration after smoothing and subtracting an L-shaped background. The experimental curve was fitted with a program that made use of combination of Gaussian–Lorentzian lines. Thermogravimetric analysis (TG/DTA) was carried out on a PCT-1A thermal analysis system produced locally. Samples with mass of about 10.0 mg were heated in air at a heating rate of 5 °C/min to a maximum temperature of 1100 °C.

2.3. Catalytic reaction

Catalytic wet oxidation of phenol was used as a probe reaction to examine the catalytic performance of the calcined products. Hydrogen peroxide solution (0.2 mL) was added rapidly to a magnetically stirred aqueous phenol solution (20 mL, 100 mg/L) containing the catalyst (0.04 g) in a 50 mL conical flask. The reaction was carried out at 25 °C for 1 h with vigorous agitation and, after removal of the heterogeneous catalyst by filtration, the liquid was then analyzed by high performance liquid chromatography (HPLC) (Shimadzu LC-10AT). The initial and final concentrations of phenol were measured. Aliquots (5 μL) were injected into a reverse-phase C-18 column, with a mixture of 30% methanol and 70% redistilled water as a mobile phase at a total

flow rate of 0.8 mL/min. The absorbance at 280 nm was used to measure the concentration of phenol.

3. Results and discussion

3.1. Preparation and characterization of Ce-containing LDH precursors

Since the presence of Al^{3+} is responsible for the positive charge on the layers, the theoretical anion exchange capacity of the Cu-LDH for the trivalent guest anions corresponds to a $[Ce(dipic)_3]^{3-}$/Al molar ratio of 1/3. Elemental analysis for the CuCe-LDH sample gives a Ce/Al molar ratio of 1/3.7, only slightly lower than the theoretical value, suggesting the nearly complete intercalation of $[Ce(dipic)_3]^{3-}$ anions into the host LDH. The calculated structural formula of the CuCe-LDH material is $[Cu_{0.33}Zn_{0.30}Al_{0.37}(OH)_2][Ce(dipic)_3^{3-}]_{0.10}(CO_3^{2-})_{0.03}\cdot 0.61H_2O$, assuming that the charge balance is made up by the intercalation of a small amount of CO_3^{2-} into the interlayer galleries; such contamination is commonly observed for LDHs [30].

The XRD pattern of CuCe-LDH displays the typical diffraction lines of a LDH phase (Fig. 1a) [31]. The basal (0 0 3) reflection is shifted to a lower angle compared with Cu-LDH (Fig. 1c), indicating an increase in basal spacing to 1.28 nm as a result of the replacement of nitrate anions in the LDH interlayer galleries by the larger $[Ce(dipic)_3]^{3-}$ anions. Furthermore, weak reflections characteristic of a CO_3^{2-}-LDH phase are also observed, confirming the contamination by carbonate suggested by elemental analysis. Fig. 1b displays the XRD pattern of CuCe-LDH with an initial $[Ce(dipic)_3]^{3-}$/Al ratio of 1/6, lower than the stoichiometric ratio for complete intercalation of the complex. The similar basal spacing of 1.28 nm suggests the presence of a $[Ce(dipic)_3]^{3-}$-intercalated LDH crystals. As expected, since the initial amount of $[Ce(dipic)_3]^{3-}$ is less than the anion exchange capacity, the characteristic reflections of the residual NO_3^--LDH phase are also clearly observed.

Subtracting the layer thickness (0.48 nm) from the experimental basal spacing of CuCe-LDH gives a gallery height of 0.80 nm. Based on the single crystal X-ray structure of the $[Nd^{III}(dipic)_3]^{3-}$ sodium salt [32], which is isomorphous with the cerium analog with a very similar unit cell size, the $O_2\ldots O_4$ distance parallel to the C_3 axis in $[Ce^{III}(dipic)_3]^{3-}$ is estimated to be about 0.508 nm (Fig. 2a). Taking into account the van der

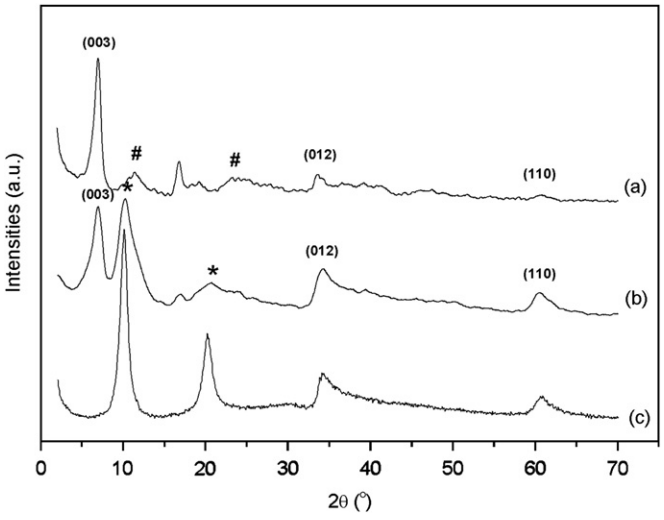

Fig. 1. XRD patterns of CuCe-LDH samples with different initial $[Ce(dipic)_3]^{3-}$/Al ratios of 1/1 (a), 1/6 (b), and Cu-LDH (c) (#: CO_3-LDH; *: NO_3-LDH).

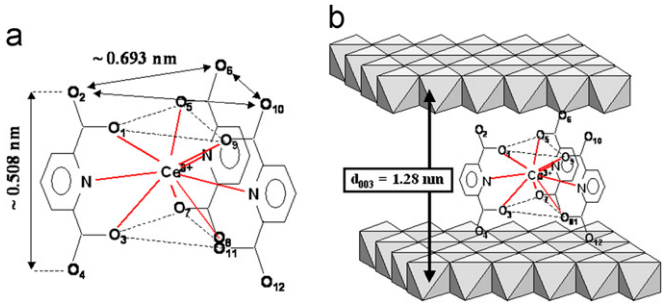

Fig. 2. Representation of the suggested interlayer arrangement of $[Ce(dipic)_3]^{3-}$ anions in interlayer galleries of LDH.

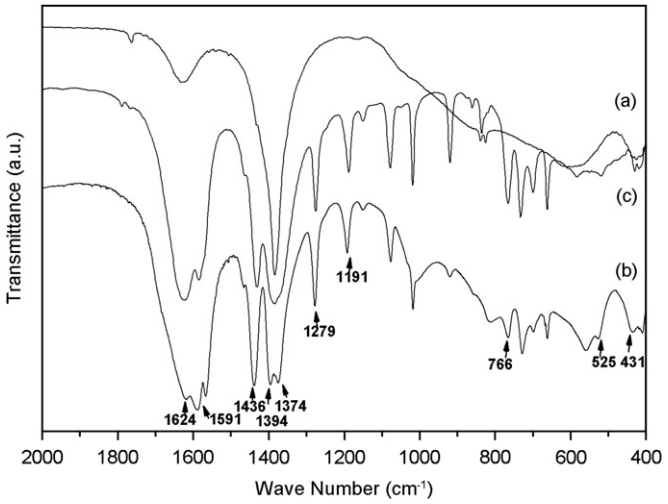

Fig. 3. FT-IR spectra of Cu-LDH (a), CuCe-LDH (b) and $Na_3[Ce(dipic)_3]\cdot xH_2O$ (c).

Waals radius of oxygen (0.153 nm), the length of $[Ce^{III}(dipic)_3]^{3-}$ anion along its C axis is about 0.814 nm, very similar to the observed gallery height. This suggests that the $[Ce^{III}(dipic)_3]^{3-}$ anions are oriented with their C_3 axes perpendicular to the layers in the interlayer galleries of LDH (Fig. 2b). Such an orientation allows the guest anions to maximize the hydrogen bonding interactions with both adjacent layers [33].

The FT-IR absorption spectrum of CuCe-LDH is shown in Fig. 3b. The bands observed in the low-frequency region 400–900 cm^{-1} correspond to the lattice vibration modes of the LDH structure [2]. The majority of the characteristic bands in the region 1000–1800 cm^{-1} are similar to those of $Na_3[Ce(dipic)_3]\cdot xH_2O$ (Fig. 3c). The bands at 1591, 1436, 1279 and 1191 cm^{-1} correspond to the vibrations of the skeletal modes of the pyridine ring [34]. The intense absorption bands at about 1624 and 1374 cm^{-1} in the spectrum of CuCe-LDH can be assigned to asymmetric ν_{as}(OCO) and symmetric ν_s(OCO) stretching vibrations, respectively, of the carboxylate groups. The corresponding carboxylate stretching vibrations of free $Na_3[Ce(dipic)_3]\cdot xH_2O$ occur at about 1614 and 1392 cm^{-1}. The changes in peak positions and $\Delta\nu$ (ν_{as}(OCO)–ν_s(OCO)) after intercalation may be explained by the electrostatic attraction between the $[Ce(dipic)_3]^{3-}$ complexes and the positively charged metal hydroxyl layers. The IR spectrum is therefore consistent with the formation of the $[Ce(dipic)_3]^{3-}$-intercalated LDH network. The weak vibration expected at $\sim$1365 cm^{-1} from the small amount of CO_3^{2-} impurity may be masked by the symmetric carboxylate stretching vibration of the $[Ce(dipic)_3]^{3-}$ anions.

The Cu–Ce–O mixed oxides were obtained by controlled thermal decomposition of the CuCe-LDH precursors. Thermal treatment of LDHs results in the formation of mixed oxides whose

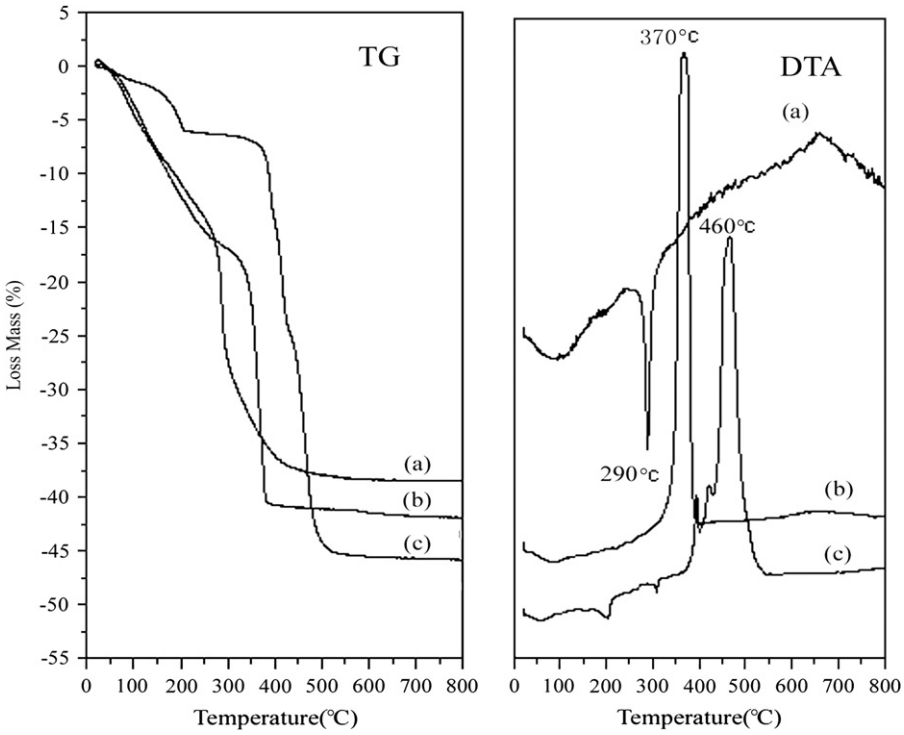

Fig. 4. TG–DTA curves for Cu-LDH (a), CuCe-LDH (b) and $Na_3[Ce(dipic)_3]\cdot xH_2O$ (c).

phase and crystallinity are mainly influenced by the chemical composition of the precursor and the calcination temperature [35]. The TG–DTA curves of CuCe-LDH and Cu-LDH in air are illustrated in Fig. 4, and Fig. 5 shows in situ variable temperature XRD patterns of two samples from room temperature up to 1025 °C. The weight-loss stages of CuCe-LDH (Fig. 4b) are in good agreement with those generally reported in the literature for LDH materials [3,36]. Remove of surface adsorbed and interlayer structural water and dehydroxylation of brucite-like layers result in the minor weight-loss stage below 280 °C, with a weight loss of 17%. The DTA curve shows small and broad endothermic peaks at the stage. The in situ XRD patterns (Fig. 5b) indicate that loss of the hydrogen bonding network results in a decrease in the order of the guest anions, reflected in the reduced intensity of the (0 0 3) reflection. The major weight-loss stage, in the region 280–390 °C, can be attributed to the decomposition/combustion of $[Ce(dipic)_3]^{3-}$ ions and dehydroxylation of a few residual *M*–OH groups, and is accompanied by a strong exothermic effect at about 370 °C in the DTA curve. The total weight loss for the Ce-containing LDH is ca. 42%. As shown in the XRD patterns above 350 °C, the characteristic LDH peaks disappear almost completely at these temperatures, suggesting that an amorphous oxide phase has been formed. When the temperature is increased to 600 °C, crystallization of highly disordered metal oxides (ZnO, CuO) is observed. Moreover, the characteristic reflections of CeO_2 are also present. Above 800 °C, the characteristic peaks of mixed spinel phases ($ZnAl_2O_4$, $CuAl_2O_4$) appear. For the Ce-free LDH, as shown in Fig. 4a, the major weight loss is observed between 240 and 320 °C with a large endothermic effect at about 290 °C, resulting from decomposition of the interlayer NO_3^- anions and partial dehydroxylation of the brucite-like layers. This is consistent with the in situ XRD data (Fig. 5a), which show that the complete collapse of the LDH layers occurs at 250 °C. The crystallization of disordered metal oxides begins above 550 °C, and a mixture of crystallized oxides and spinels is observed at 700 °C [37]. The crystallization temperatures for the different components arising from the decomposition of CuCe-LDH are therefore higher than those for the corresponding products arising from the decomposition of Cu-LDH. As a result, the amount and particle size of $CuAl_2O_4$ and $ZnAl_2O_4$ spinel phases arising from decomposition of CuCe-LDH are lower at a given temperature, which is desirable from the point of view of catalysis. Other researchers have also reported [12,20] that CuO–CeO_2 mixed oxides prepared in other ways can inhibit the formation of spinel phases and improve the thermal stability of divalent metal oxides. It should be noted that the thermal stability of the intercalated complex is lower than that in free $Na_3[Ce(dipic)_3]\cdot xH_2O$ (about 460 °C). This may be the result of the perturbation of the carboxylate groups coordinated to Ce^{3+} induced by the interaction with the LDH layers, as illustrated in Fig. 3. An alternative explanation is that the structure of $Na_3[Ce(dipic)_3]\cdot xH_2O$ consists of a strongly hydrogen-bonded network of hydrated cations and anions [38], and this is lost when the complex is dispersed in the interlayer galleries.

3.2. Structural and catalytic properties of Ce-containing mixed oxides

Nitrogen adsorption/desorption experiments were carried out in order to determine the specific surface areas and pore size distributions of the Cu–Ce–O mixed oxides derived from CuCe-LDH. As illustrated in Fig. 6A, Cu-500-6, CuCe6-500-6 and CuCe-500-6 all show isotherms typical of type IV in the IUPAC classification, indicative of mesoporous materials. The shapes of the hysteresis loops differ however, suggesting that different pore characteristics are present. As the Ce content increases, the hysteresis loops become increasingly narrow in the high pressure region, indicating that some micropores are present in addition to the mesopores [39]. Fig. 6B illustrates a comparison between the pore size distributions of the Ce-containing and Ce-free materials after calcination at 500 °C for 6 h. CuCe-500-6 shows a maximum in the region 3–5 nm, as well as a broad and low peak below 2 nm. Its mesoporosity is more uniform than Cu-500-6, suggesting a decrease in the irregular stacking of oxide particles.

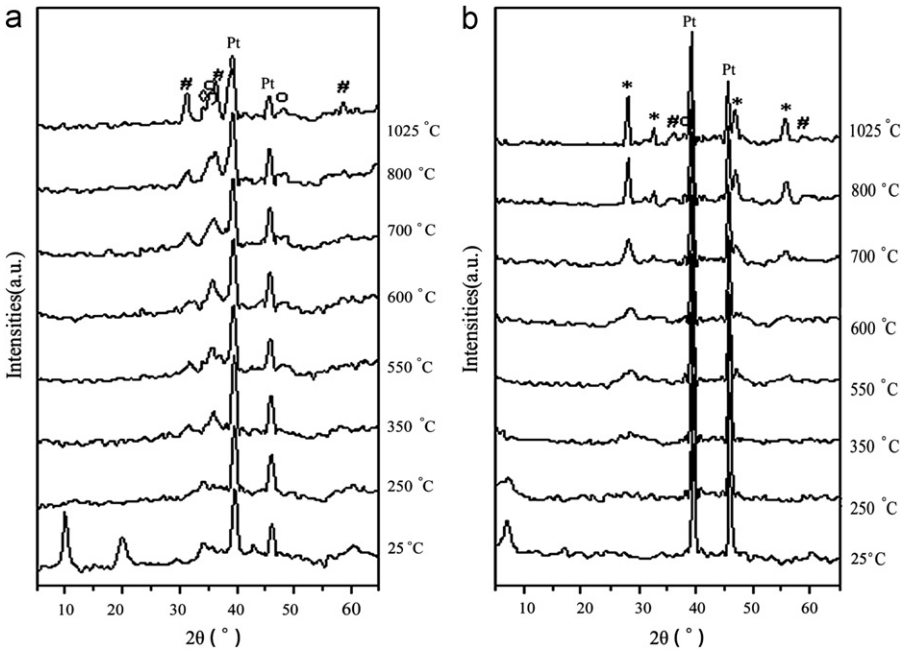

Fig. 5. *In situ* variable temperature XRD patterns of Cu-LDH (a) and CuCe-LDH (b) (#: $CuAl_2O_4$; ○:CuO; ◇:ZnO; *:CeO_2; Pt signals come from the experimental substrates).

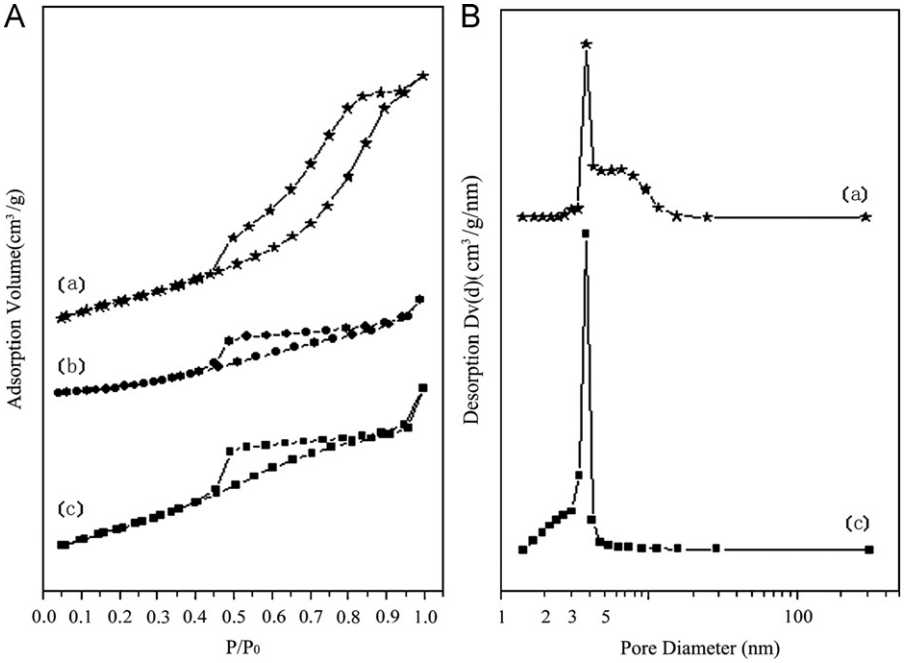

Fig. 6. N_2 adsorption–desorption isotherms (A) and pore size distribution curves (B) of Cu-500-6 (a), CuCe6-500-6 (b), and CuCe-500-6 (c).

The narrow pore size distribution of the Ce-containing materials should enhance catalytic properties.

The Cu–Ce–O mixed oxides prepared from different CuCe-LDH precursors show their maximum specific surface areas at a calcination temperature of 500 °C, consistent with the previous reports for other LDH materials [40,41]. At 500 °C, the layered structure is completely destroyed, giving rise to mixed metal oxides, but the mesoporous properties are still retained. The specific surface area of the calcined CuCe-LDH (47.6 m^2/g for CuCe-500-6) is slightly smaller than that of the Ce-free analog (51.4 m^2/g for Cu-500-6). The decomposition of $[Ce(dipic)_3]^{3-}$ anions generates NO/NO_2, CO_2 and H_2O, and the release of these volatile species produces many channels (as confirmed in Fig. 6), which tends to increase the specific surface area [42]. On the other hand, the formation of Cu–Ce–O composite oxides leads to decrease in the specific surface area. These two opposing factors roughly cancel one another out, and there is only a small change in the specific surface area. The specific surface area also depends on the initial Ce/Al ratio. For CuCe6-500-6 (24.7 m^2/g), the amount of $[Ce(dipic)_3]^{3-}$ anions is insufficient for complete ion exchange, and the decreased number of channels generated by the loss of volatile species results in an obvious reduction in the specific surface area. The specific surface area is also influenced by calcination time: the surface area decreases from 38.4 m^2/g for CuCe6-500-3 to 24.7 m^2/g for CuCe6-500-6 as the calcination time increases, which can be mainly attributed to the formation

of a larger amount of Cu–Ce–O composite oxides after an extended calcination process.

Phenol oxidation by hydrogen peroxide was carried out as a probe reaction to investigate the catalytic performance of the Cu–Ce–O mixed oxides, and the phenol conversions are listed in Table 2. The conversions increased significantly with increasing Ce contents in catalysts obtained under the same calcination conditions (either 500 °C/6 h or 500 °C/3 h), with CuCe-500-6 showing the highest catalytic activity (35.9%), approximately three times that of the Ce-free Cu-500-6 (12.2%). It is noteworthy that although the specific surface area of CuCe-500-6 is lower than that of Cu-500-6, the activity of the former is much higher, which implies that the Cu–Ce interactions in the as-synthesized Cu–Ce–O mixed oxides play a more important role than specific surface area in determining catalytic activity. The effects of varying the calcination time and temperature were also studied. The phenol conversions increase with increasing calcination time from 3 h to 6 h, and the change is more significant for the series of catalysts with higher Ce contents. This suggests that a longer calcination process favors the formation of Cu–Ce–O mixed oxides, and the resulting enhanced Cu–Ce interactions can be considered as the main factor responsible for the observed improvement in catalytic activity. The CuCe-LDH catalyst calcined at 700 °C showed a lower conversion than that calcined at 500 °C. The decreased catalytic activity is consistent with the loss of specific surface area associated with sintering at the higher calcination temperature [35]. Furthermore, the aggregation of copper clusters and crystal growth of cerium oxides on heating (as shown in Fig. 5) lead to a reduced number of active oxygen species, which will also contribute to the decrease in catalytic activity. To further investigate the role of the Cu–Ce interactions, two kinds of physical mixtures concerning Cu-LDH, namely Physical mixture-500-6 and Cu-500-6+CeO_2, were used as control catalysts. Although the physical mixtures have a Ce/Al ratio of 1/3, the observed phenol conversions were almost equal to that obtained with Cu-500-6, and much lower than that obtained with CuCe-500-6. This suggests that the absence of Cu–Ce interactions has a significant adverse effect on catalytic activity. It is proposed that the improvement in catalytic performance of the Cu–Ce–O mixed oxides is mainly attributed to the Cu–Ce interactions induced on heating only when Ce ions in $[Ce(dipic)_3]^{3-}$ forms are intercalated into the layered structure, which is probably related to a uniform dispersion of metal ions on an atomic scale in the LDH precursors.

Table 2
Conversions of phenol obtained with calcined LDH catalysts.

Sample	Conversion of phenol (%)
Blank	4.1
Cu-500-3	11.4
Cu-500-6	12.2
Cu-700-6	9.8
CuCe6-500-3	17.8
CuCe6-500-6	22.6
CuCe-500-3	20.7
CuCe-500-6	35.9
CuCe-700-6	26.2
Cu-500-6+CeO_2	13.3
Physical mixture-500-6	10.2

Phenol: 20 ml, 100 mg/L; catalyst: 0.04 g; H_2O_2: 0.2 ml; 25 °C and room pressure; time: 1 h.

3.3. Mechanism for catalysis by Cu–Ce–O mixed oxides

In phenol oxidation using Cu-based catalysts, the major active centers have been found to be copper clusters which provide surface sites for the reaction of phenol [43]. Because the pore size of the calcined LDH materials is larger than the size of the phenol molecule (<0.5 nm) the diffusion step should be fast, and either the adsorption or the reaction step should be rate limiting in this catalytic process. Thus the catalytic activity principally depends on the degree of dispersion of the metal oxides, the spatial orientation of the phenol molecules, the chemical state of the active sites and the amount of active oxygen moieties. For Cu-500-6, which does not contain any Ce, copper oxides are uniformly and densely packed on the catalyst surface, so that the adsorption sites of phenol molecules may be close together which partially inhibits the reaction step. For CuCe-LDH materials, however, the ion-exchange process with the $[Ce(dipic)_3]^{3-}$ anions affords a uniform dispersion of Ce ions in the LDH interlayer galleries owing to the network of supramolecular host–guest interactions. After calcination, the resulting Cu–Ce–O mixed oxides can inherit the high dispersion of metal cations in the LDH precursor due to the topotactic nature of the thermal decomposition reaction [31]. The uniform distribution of Ce ions may reduce the number of Cu sites per unit surface area, increase the short-range ordering, and thus possibly promote the effective adsorption of phenol molecules, all of which enhance the catalytic efficiency of Cu ions, as previously proposed by Velu et al. [44].

Furthermore, the other important advantage of the Cu–Ce–O mixed oxides is the presence of the Cu–Ce interactions. It has been reported that Cu–Ce interactions can significantly modify the low-temperature copper redox activity and the lattice oxygen lability [15,45,46]. The high oxygen storage capacity and abundant lattice defects, such as oxygen vacancies, in cerium oxides are known to favor the formation of reactive oxygen species [20,21]. In order to determine the effect of cerium on the chemical states of copper and oxygen in the Cu–Ce–O mixed oxides derived from $[Ce(dipic)_3]^{3-}$-intercalated LDHs, Cu-500-6, CuCe6-500-6 and CuCe-500-6 were analysed by XPS. The Cu $2p_{3/2}$ XPS data are listed in Table 3. For the Ce-free sample, two main peaks are observed at 934.8 and 933.1 eV, attributed to Cu^{2+} cations in $CuAl_2O_4$ (A) and CuO (B) structures, respectively [40]. For the two Ce-containing samples, in addition to these two peaks, two additional peaks are present, demonstrating that the presence of cerium modifies the chemical environment of copper. One additional peak at around 934.3 eV is in the range

Table 3
XPS characteristics of Cu $2p_{3/2}$ regions for calcined LDH samples.

Sample	Binding energy (eV)				Peak intensity[b] (%)			
	Cu^+	Cu_B^{2+} (Cu–O)	Cu_C^{2+} (Cu–Ce–O)	Cu_A^{2+} (Spinel)	$I(Cu^+)$	$I(Cu_B^{2+})$	$I(Cu_C^{2+})$	$I(Cu_A^{2+})$
Cu-500-6	–	933.1 (2.8)[a]	–	934.8 (2.5)	–	76.4	–	23.6
CuCe6-500-6	932.4(2.5)	933.2 (2.6)	934.2 (2.2)	935.0 (2.8)	30.7	38.7	23.0	7.6
CuCe-500-6	932.1(2.2)	933.0 (1.7)	934.3 (1.9)	934.9 (2.7)	39.4	31.0	25.1	4.5

[a] Numbers in parentheses refer to full width at half-maximum (FWHM) in eV.
[b] Intensity of the peak as a percentage of the total Cu $2p_{3/2}$ area.

Table 4
XPS characteristics of Ce $3d_{5/2}$ regions for calcined LDH samples.

Sample	Binding energy (eV)			Peak intensity[a] (%)		
	Ce^{3+}	Ce_A^{4+} (Ce–O)	Ce_B^{4+} (Cu–Ce–O)	$I(Ce^{3+})$	$I(Ce_A^{4+})$	$I(Ce_B^{4+})$
CuCe6-500-6	881.0 (1.9)	882.2 (2.0)	884.0 (2.4)	13.9	53.2	32.9
CuCe-500-6	881.0 (1.8)	882.3 (1.8)	883.9 (2.5)	13.5	48.5	38.0

[a] Intensity of the peak as a percentage of the total Ce $3d_{5/2}$ area.

Table 5
XPS characteristics of O 1*s* regions for calcined LDH samples.

Sample	Binding energy (eV)			Peak intensity[a] (%)	
	O_I (O–*M*′)	O_I (O–*M*)	O_{II} (O–H)	$I(O_I)$	$I(O_{II})$
Cu-500-6	–	529.2 (3.0)	531.2 (3.0)	35.3	64.7
CuCe6-500-6	526.7(2.7)	529.3 (2.1)	531.1 (2.6)	57.2	42.8
CuCe-500-6	526.5(2.5)	529.2 (1.9)	531.2 (2.5)	63.2	36.8

[a] Intensity of the peak as a percentage of the total O 1*s* area.

expected for Cu^{2+}, implying a new coordination environment of Cu^{2+} (C). The other, at around 932.1 eV, can be assigned to Cu^{+} on the basis of the literature [47,48], since cerium is known to increase the relative stability of Cu^{+} via electron transfer. As the Ce content increases, the relative surface atom fractions of Cu^{2+} in spinel (A) and oxide (B) sites decrease significantly, while these in Cu^{+} and Cu^{2+} (C) sites simultaneously increase and thus become the major components. This may be attributed to the strong influence of adjacent Ce centers on Cu centers through the Cu–Ce interactions. The XPS characteristics of Ce $3d_{5/2}$ are shown in Table 4. Three peaks are observed for both Ce-containing samples. The peaks at around 882.3 and 883.9 eV can be assigned to two kinds of Ce^{4+} species (V_0 peak) [49], corresponding to ceria (A) and Cu–Ce–O mixed oxide (B) phases, respectively [47]. The third peak at around 881.0 eV can be assigned to Ce^{3+} cations [49], suggesting a partial reduction of the Ce(IV) ions in the precursor. As the Ce content increases, the proportions of the two types of Ce^{4+} show a significant variation: the number of Ce^{4+} (A) decreases whilst that of Ce^{4+} (B) increases, consistent with the formation of a larger amount of a Cu–Ce–O mixed oxide phase. XPS analysis thus unambiguously confirms the presence of Cu–Ce interactions in the calcined CuCe-LDH materials. These interactions are expected to have a positive influence on the catalytic ability of the Cu–Ce–O materials because they modify the chemical states of Cu sites and stabilize the more catalytically active Cu^{+} sites [21,46] relative to Cu^{2+}. It has been proposed [50] that the following redox equilibrium may occur during calcination processes:

$$Ce^{3+} + Cu^{2+} \rightarrow Ce^{4+} + Cu^{+}$$

and since the ionic radius of Cu^{+} (0.115 nm) is close to that of 8-coordinate Ce^{4+} (0.092 nm) the formation of Cu–Ce–O mixed oxides by isomorphous substitution occurs readily.

The O 1*s* XPS spectra of the three samples display two different kinds of surface oxide species, denoted O_I and O_{II}, whose relative abundances are listed in Table 5. The O_I peak at around 529.2 eV can be assigned to lattice oxygen bound to metal cations [40], and the other O_I peak with lower binding energy at around 526.5 eV may result from lattice oxygen in the Cu–Ce–O mixed oxides, whilst the O_{II} peak at around 531.2 eV can be assigned to surface oxygen sites, mainly as hydroxyl groups. The proportion of O_I increases significantly with increasing Ce content and the abundant lattice oxygen may also contribute to the observed enhanced catalytic ability of the Cu–Ce–O materials [47].

4. Conclusion

$[Ce(dipic)_3]^{3-}$-intercalated Cu/Zn/Al LDH materials and their calcined derivatives, Cu–Ce–O mixed oxides, have been synthesized, and their textural and structural properties characterized by a variety of physicochemical techniques. The results indicate that the as-synthesized LDH materials have a hydrotalcite-like layered structure with the $[Ce(dipic)_3]^{3-}$ anions intercalated in the interlayer galleries. Subsequent calcination leads to the formation of the Cu–Ce–O mixed oxides. The presence of cerium is found to influence the thermal stability, pore structure, specific surface area and chemical state of the resulting oxide materials. Furthermore, the catalytic performance of the Cu–Ce–O mixed oxides in aqueous phenol oxidation was superior to that of Ce-free analogs. It is proposed that the Cu–Ce interactions which result after calcination are the main factor responsible for the significant enhancement in catalytic activity of the Cu–Ce–O mixed oxides.

Acknowledgment

This work was supported by the National Science Foundation of China, the 973 Program (2011BAC06B09), the 111 Project (B07004), and the Scientific Research Foundation for the Returned Overseas Chinese Scholars State Education Ministry.

References

[1] G.R. Williams, D. O'Hare, J. Mater. Chem. 16 (2006) 3065–3074.
[2] D.G. Evans, R.C.T. Slade, Struct. Bonding 119 (2006) 1–87.
[3] L.H. Zhang, F. Li, D.G. Evans, X. Duan, Mater. Chem. Phys. 87 (2004) 402–410.
[4] J.J. Yu, X.P. Wang, Y.X. Tao, Z.P. Hao, Z.P. Xu., Ind. Eng. Chem. Res. 46 (2007) 5794–5797.
[5] Z.G. Xiong, Y.M. Xu, Chem. Mater. 19 (2007) 1452–1458.
[6] S. Bhattacharjee, T.J. Dines, J.A. Anderson, J. Phys. Chem. C 112 (2008) 14124–14130.
[7] H. Wang, X. Xiang, F. Li, D.G. Evans, X. Duan, Appl. Surf. Sci. 255 (2009) 6945–6952.
[8] S. Pande, A. Saha, S. Jana, S. Sarkar, M. Basu, M. Pradhan, A.K. Sinha, S. Saha, A. Pal, T Pal, Org. Lett. 10 (2008) 5179–5180.
[9] R.-M. Liou, S.-H. Chen, J. Hazard. Mater. 172 (2009) 498–506.
[10] J.-Y. Luo, M. Meng, Y.-Q. Zha, L.-H. Guo, J. Phys. Chem. C 112 (2008) 8694–8701.
[11] X.-J. Guo, L.-M. Li, S.-M. Liu, G.-L. Bao, W.-H. Hou, J. Fuel Chem. Technol. 35 (2007) 329–333.
[12] S. Velu, K. Suzuki, Top. Catal. 22 (2003) 235–244.
[13] M.F. Luo, Y.P. Song, J.Q. Lu, X.Y. Wang, Z.Y. Pu, J. Phys. Chem. C 111 (2007) 12686–12692.
[14] F. Arena, R. Giovenco, T. Torre, A. Venuto, A. Parmaliana, Appl. Catal. B: Environ. 45 (2003) 51–62.
[15] J.A. Dyakonov, D.A. Grider, B.J. McCormick, P.K. Kahol, Appl. Catal. A: Gen. 192 (2000) 235–246.
[16] P. Djinovic, J. Batista, A. Pintar, Appl. Catal. A: Gen. 347 (2008) 23–33.
[17] I. Chen, S. Lin, C. Wang, L. Chang, J. Chang, Appl. Catal. B: Environ. 50 (2004) 49–58.
[18] M. Jobbagy, F. Marino, B. Schonbrod, G. Baronetti, M. Laborde, Chem. Mater. 18 (2006) 1945–1950.
[19] X.C. Zheng, X.L. Zhang, Z.Y. Fang, X.Y. Wang, S.R. Wang, S.H. Wu, Catal. Commun. 7 (2006) 701–704.
[20] M. Ferrandon, B. Ferrand, E. Bjornbom, F. Klingstedt, A.K. Neyestanaki, H. Karhu, I.J. Vayrynen, J. Catal. 202 (2001) 354–366.
[21] P.G. Harrison, I.K. Ball, W. Azelee, W. Daniell, D. Goldfarb, Chem. Mater. 12 (2000) 3715–3725.
[22] P. Bera, K.R. Priolkar, P.R. Sarode, M.S. Hegde, S. Emura, R. Kumashiro, N.P. Lalla, Chem. Mater. 14 (2002) 3591–3601.

[23] J. Das, D. Das, K.M. Parida, J. Colloid Interf. Sci. 301 (2006) 569–574.
[24] S. Gago, M. Pillinger, R.A.S. Ferreira, L.D. Carlos, T.M. Santos, I.S. Goncalves, Chem. Mater. 17 (2005) 5803–5809.
[25] I. Cota, E. Ramírez, F. Medina, E.S. Jesús, G. Layrac, D. Tichit, Appl. Catal. A: Gen. 382 (2010) 272–276.
[26] Z. Chang, D.G. Evans, X. Duan, P. Boutinaud, M. de Roy, C. Forano, J. Phys. Chem. Solids 67 (2006) 1054–1057.
[27] L. Sarakha, C. Forano, P. Boutinaud, Opt. Mater. 31 (2009) 562–566.
[28] S. Miyata, Clays Clay Miner. 31 (1983) 305–311.
[29] G.R. Choppin, P.A. Baisden, S.A. Khan, Inorg. Chem. 18 (1979) 1330–1332.
[30] J. He, M. Wei, B. Li, Y. Kang, D.G. Evans, X. Duan, Struct. Bonding 119 (2006) 89–119.
[31] D.G. Evans, X. Duan, Chem. Commun. 6 (2006) 485–496.
[32] J. Albertsson, Acta Chem. Scand. 26 (1972) 1023–1044.
[33] W. Barriga, P. Jones, V. Malet, M. Rives, A. Ulibarri, Inorg. Chem. 37 (1998) 1812–1820.
[34] J. Dexpert-Ghys, C. Picard, A. Taurines, J. Incl. Phenom. Macrocyc. Chem. 39 (2001) 261–267.
[35] A. Dubey, V. Rives, S. Kannan, J. Mol. Catal. A: Chem. 181 (2002) 151–160.
[36] Q.Z. Yang, D.J. Sun, C.G. Zhang, X.J. Wang, W.A. Zhao, Langmuir 19 (2003) 5570–5574.
[37] X.F. Zhao, F.Z. Zhang, S.L. Xu, D.G. Evans, X. Duan, Chem. Mater. 22 (2010) 3933–3942.
[38] C. Li, G. Wang, D.G. Evans, X. Duan, J. Solid State Chem. 177 (2004) 4569–4575.
[39] V. Rives, Mater. Chem. Phys. 75 (2002) 19–25.
[40] F. Li., L.H. Zhang, D.G. Evans, X. Duan., Colloids Surf. A: Physicochem. Eng. Aspects 244 (2004) 169–177.
[41] F. Cavani, F. Trifiro, A. Vaccari, Catal. Today 11 (1991) 173–301.
[42] M.D. Arco, E. Cebadera, S. Gutiérrez, C. Martín, M.J. Montero, V. Rives, J. Rocha, M.A. Sevilla, J. Pharm. Sci. 93 (2004) 1649–1658.
[43] L.H. Zhang, J. Zhu, X.R. Jiang, D.G. Evans, F. Li, J. Phys. Chem. Solids 67 (2006) 1678–1686.
[44] Velu, K Suzuki, T Osaki, Catal. Lett. 62 (1999) 159–167.
[45] T. Bunluesin, E.S. Putna, R.J. Gorte, Catal. Lett. 41 (1996) 1–5.
[46] B. Wen, M.Y. He, E. Schrum, C. Li, J. Mol. Catal. A: Chem. 180 (2002) 187–192.
[47] A. Aboukais, A. Galtayries, E. Abi-Aad, D. Courcot, J. Grimblot, Colloids Surf. A: Physicochem. Eng. Aspects 154 (1999) 335–342.
[48] M. Fernandez-Garcia, E.G. Rebollo, A.G. Ruiz, J.C. Conesa, J. Soria, J. Catal. 172 (1997) 146–159.
[49] F. Larachi, J. Pierre, A. Adnot, A. Bernis, Appl. Surf. Sci. 195 (2002) 236–250.
[50] H. Stanko, J. Catal. 184 (1999) 39–48.